Microphase-Separated Elastic and Ultrastretchable Ionogel for Reliable Ionic Skin with Multimodal Sensation

Lv, Dong; Li, Xin; Huang, Xin; Cao, Chunyan; Ai, Liqing; Wang, Xuejiao; Ravi, Sai Kishore; Yao, Xi

Published in:
Advanced Materials

Published: 25/04/2024

Document Version:
Post-print, also known as Accepted Author Manuscript, Peer-reviewed or Author Final version

Publication record in CityU Scholars:
Go to record

Published version (DOI):
10.1002/adma.202309821

Publication details:
Lv, D., Li, X., Huang, X., Cao, C., Ai, L., Wang, X., Ravi, S. K., & Yao, X. (2024). Microphase-Separated Elastic and Ultrastretchable Ionogel for Reliable Ionic Skin with Multimodal Sensation. *Advanced Materials*, *36*(17), Article 2309821. https://doi.org/10.1002/adma.202309821

Microphase-separated elastic and ultrastretchable ionogel for reliable ionic skin with multimodal sensation

Dong Lv[1], Xin Li[1], Xin Huang[2], Chunyan Cao[1], Liqing Ai[1], Xuejiao Wang[1], Sai Kishore Ravi[3] and Xi Yao[1, 4]**

[1] Department of Biomedical Sciences, City University of Hong Kong, Hong Kong, 99907, P. R. China;

[2] Institute of Chemical Materials, China Academy of Engineering Physics (CAEP), Mianyang, 621900, P. R. China;

[3] School of Energy and Environment, City University of Hong Kong, Hong Kong, 99907, P. R. China;

[4] City University of Hong Kong, Shenzhen Research Institute, Shenzhen, 518075, P. R. China;

*To whom correspondence should be addressed. E-mail: xi.yao@cityu.edu.hk; skravi@cityu.edu.hk.

Keywords: bioinspired, microphase separation, ionogel, ionic skin, multimodal sensing

Abstract

Bioinspired artificial skins integrated with reliable human-machine interfaces and stretchable electronic systems have attracted considerable attention. However, the current design faces difficulties in simultaneously achieving satisfactory skin-like mechanical compliance and self-powered multimodal sensing. Here, we report a microphase-separated bicontinuous ionogel which possesses skin-like mechanical properties and mimics the multimodal sensing ability of biological skin by ion-driven stimuli-electricity conversion. The ionogel exhibits excellent elasticity and ionic conductivity, high toughness and ultrastretchability, as well as a Young's modulus similar to that of human skin. Leveraging the ion-polymer interactions enabled selective ion transport, the ionogel can output pulsing or continuous electrical signals in response to diverse stimuli such as strain, touch pressure, and temperature sensitively, demonstrating a unique self-powered multimodal sensing. Furthermore, the ionogel-based I-skin can concurrently sense different stimuli and decouple the variations of the stimuli from the voltage signals with the assistance of a machine-learning model. The ease of fabrication, wide tunability, self-powered multimodal sensing, and the excellent environmental tolerance of the ionogels demonstrate a new strategy in the development of next-generation soft smart mechano-transduction devices.

Introduction

Biological skins that integrate multi-component networks and diverse signal-transduction paths, achieve combined features of ultrastretchabiltiy and reliable multimodal sensing.[1-2] Learning from this, artificial skins derived from stretchable polymeric matrices integrated with conductive circuits that can convert external stimuli such as mechanical deformations and temperature changes into readable electrical signal, have been developed for applications in wearable sensors, human-machine systems and soft robotics.[3-7] Although various materials and technologies have been developed to improve the overall performance of ionic skins, there are still limited breakthroughs on the integration of self-powered multimodal sensing.[8] Existing multimodal sensors, which depend on piezoresistive and capacitive modes, require an additional energy source to power the sensing units, thereby complicating the integration of the device.[9-15] Recently, a force-induced current generation has been reported in hydrogels, which can generate pulsing or continuous ionic current for sensing like that in biological systems.[16-17] Yet, the poor environmental tolerance of hydrogels limits their life-span in harsh environmental conditions.[18-20]

Ionogels, in which polymer network is swollen with ionic liquid (IL), provide an alternative to hydrogels for preparing ionic conductors due to their intrinsic ionic conductivity, non-volatility and good thermal and electrochemical stability.[21-23] Nevertheless, to date, the ionic analogs of piezo-generators employing ionogels have rarely been reported. A significant challenge for exploring ionogel-based skin-like sensors is their unsatisfied mechanical and electrical properties, especially towards elasticity (<100% strain), stretchability (<2000%), strength (<1 MPa) and ionic conductivity (<0.01 mS/cm). These limitations would result in low sensitivity,

failure of signal reproduction and poor durability.[24-26] One commonly used strategy to enhance polymer gels is the incorporation with dynamic noncovalent bonds such as hydrogen bonds. However, the screening effect of IL on dynamic bonds enables ionogels with low strength and inferior elasticity.[27-30] Building abundant physical energy dissipative structures has been demonstrated as an effective way to prepare elastic and tough ionogels.[31-34] For example, phase separation method has been used in engineering ionogels with high toughness.[35-37] However, those prepared ionogels show limited elasticity and can barely recover from high strains, and their overall performances are not optimized for skin-based applications.[38] The existing ionogel-based sensors are limited by small working range, single response mode and the ability to achieve self-powered sensing.[39] Therefore, it is still a great challenge to develop ionogels with a comprehensive performance in multifunctionality for next generation of self-powered ionic skin (I-skin).

In human skin, dermis has extracellular matrix composed of collagen fibrils, microfibrils, and elastic fibers, embedded in hyaluronan and proteoglycans, which enables the human skin with tensile strength and elasticity. Meanwhile, the abundant mechanoreceptors on dermis provide the sense of touch and heat through stimuli-induced selective ion diffusion (Figure 1a).[40] Drawing inspiration from the structure-induced mechanical improvement and ion transport-induced multimodal sensing ability of human skin, we report here the fabrication of poly(vinylidene fluoride-co-chlorotrifluoroethylene) (PVDF-co-CTFE)-based ionogels which show skin-like mechanical properties and ability for self-powered multimodal sensing. The ionogel is microphase-separated and has a bicontinuous structure consisting of an IL-rich domain and a polymer-rich domain which can provide effective energy dissipation during

deformation (Figure 1b). Consequently, the prepared ionogel showed unique properties including high elasticity, ultra-stretchability, high ionic conductivity and a Young's modulus similar to human skin. The cations and anions from the IL interact differently with the copolymer matrix, and when stimulated, the spatial distribution of counterions within the ionogel changes significantly, resulting in an ionic current. Enabled by the superior mechanical properties, the fabricated ionogel-based I-skin can sensitively and reliably respond to various stimuli such as strain, pressure, and temperature in a self-powered manner. Moreover, a proficiently trained machine learning (ML) model can effectively disentangle the combined and intricate response signals produced by various stimuli concurrently. This capability empowers the I-skin to accurately and simultaneously monitor both applied pressure and temperature with precision. The ionogel also presented excellent environmental and solvents resistance which further improve its stability and durability in practical applications. Our work offers a new elastic ionogel platform for self-powered and reliable sensing in wearable devices.

Results and discussion

Design of bioinspired elastic and ultrastretchable I-skin

The design principle of the ionogel is to utilize IL that can partially swell the polymer matrix in which the polymer segments would gradually crystalize for physical crosslinking along with solvent evaporation. The copolymer of PVDF-co-CTFE was selected for demonstration due to its inherent high stretchability, low modulus, and abundant polar groups, which allow for the creation of ionogels with superior overall mechanical properties. Simultaneously, the elasticity of PVDF-co-CTFE provides an elastic force that can regulate and stabilize microphase

separation.[41] We then selected ILs with imidazolium cations due to their high ionic strength and high electrochemical stability.[42] To investigate the effect of different counterions on the properties of ionogels, six different room-temperature ILs with different cations and anions were employed (Table S1). When hydrophilic IL of 1-metyl-3-octhylimidazolium chloride (OMIMCl) was used, the solution is turbid and easy to precipitate. Ionogles produced by 1-butyl-3-octhyl imidazolium tetrafluoroborate ($OMIMBF_4$), 1-methyl-3-octyl-imidazolium-hexafluorophosphate ($OMIMPF_6$), 1-octyl-3-methylimidazolium bis(trifluoromethanesulfonyl) imide (OMIMTFSI) and 1-ethyl-3-methylimidazolium tetrafluoroborate ($EMIMBF_4$) showed poor transparency, indicating the poor compatibility between these ILs and the copolymer (Figure S1). The transmittance of the ionogels indicated that decrease in the alkyl chain length of cations or more fluorine polar groups in anions can promote the compatibility of IL with the copolymer. Transparency ionogel can be obtained with highly conductive EMIMTFSI, revealing the relatively good compatibility between EMITFSI and the copolymer which can enable the moderate microphase separation (Figure 1b).

By tuning IL contents, PVDF-co-CTFE ionogels with different mechanical and electrical properties were fabricated which were termed as PIG-x (x represents weight percentage of IL). As shown in Figure 1c, the PIG displayed good transparency in visible wavelengths with average transmittance ranges from 92% (PIG-10) to 83% (PIG-40). The ionogel is mechanically strong that a typical PIG-40 sample with ~500 μm thickness can withstand a weight of 1 kg (Figure 1d). Interestingly, the PIG showed outstanding resilience to deformation. For instance, the PIG-40 sample can fully recover from an elongation of 500% after 10 min

recovery (Figure 1e and Figure S2). Such good elasticity showed the great potential for exploring reliably bionics skin to achieve stable and repeatable sensing.

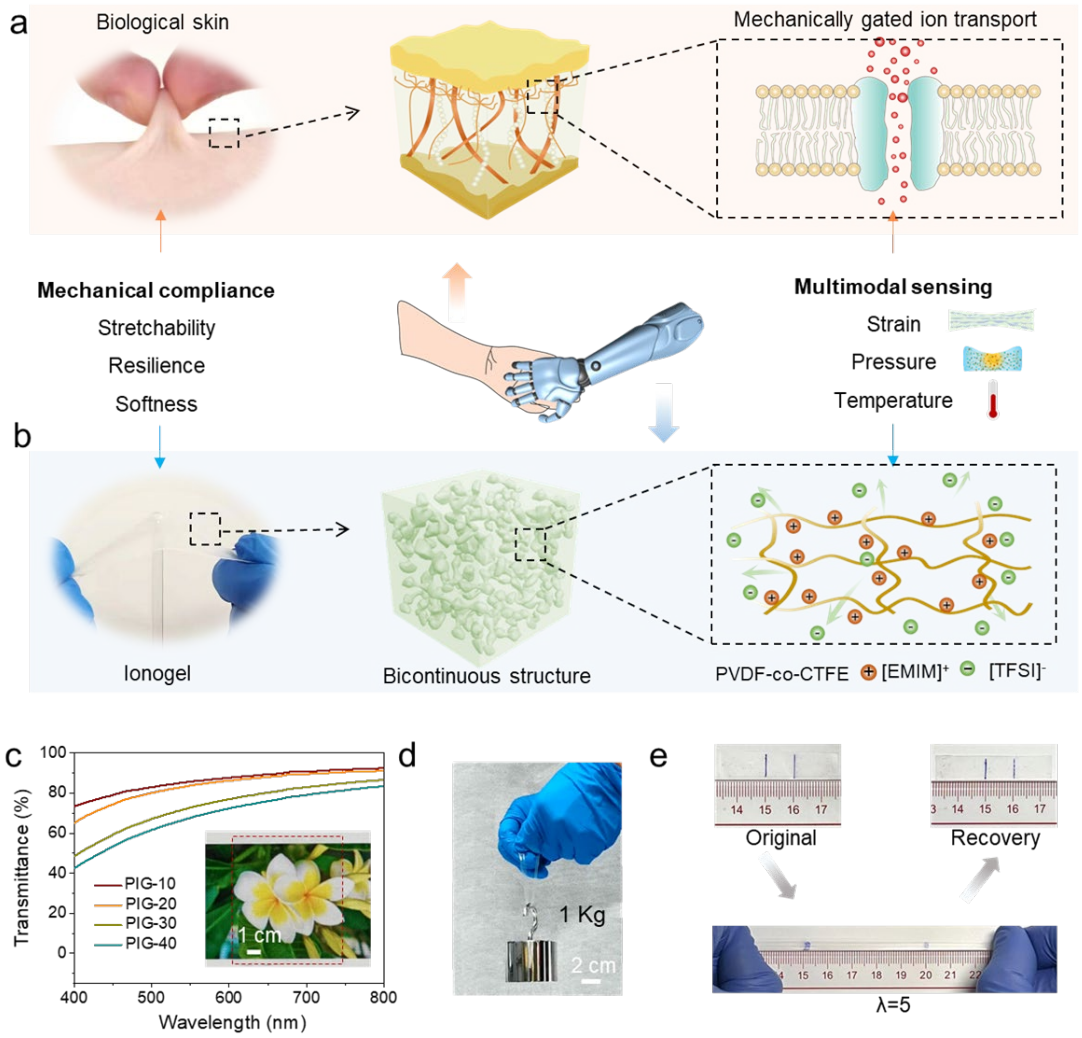

Figure 1. Design of the bioinspired PIG-based I-skin. (a) Schematic illustration of soft, elastic, and stretchable biological skins with multimodal sensing via mechanically gated ion transport. (b) Schematic illustration of the elastic and ultrastretchable PIG-based I-skin with selective ion-diffusion upon external stimuli. (c) Transmittance spectrum of PIG in the visible wavelengths. Inset: Photo of PIG-40, suggesting its high transparency. Sample size: 20×10× 0.2 mm (length, width and thickness). (d) Digital image showed that PIG-40 can hold a 1 kg weight. (e) Digital images for PIG-40 that can restore to its original length in 10 min from an elongation of 500% (thickness: 200 μm).

Microphase separation and mechanical properties of PIG

Scanning electron microscopy (SEM) images gave intuitive evidence to the microstructure evolution within the ionogels (Figure 2a and S3). All the samples exhibited a biphasic structure that significantly evolved as the IL content increased. For PIG-10, one phase of the ionogel exhibits a discrete ellipsoid morphology, which transforms into a bicontinuous structure in PIG-40. Meanwhile, transitional morphologies were observed in PIG-20 and PIG-30. To investigate the composition of the two phases, 2D Raman spectrum mapping was conducted. As shown in Figure 2b and S4, one phase prominently displays the signal of the copolymer, while the other primarily shows the signal of the anion from IL. In addition, the signal for the copolymer and IL can be found in the two phases, albeit with varying intensities in different phases. These findings suggest the simultaneous presence of a polymer-rich phase and an IL-rich phase in PIG (Figure 2c). The biphasic structure with polymer-rich phase and IL-rich phase was also confirmed by Energy Dispersive X-Ray (EDX) mapping (Figure S5). The stacks of fluorescence confocal images showed that the three-dimensional (3D) structure of the IL-rich phase in PIG-40 is continuous and microphase-separated, further indicating that PIG-40 has a bicontinuous structure (Figure 2d). From the 3D confocal image, the diameter of the continuous IL-rich phase is ~3 μm which is consistent with the SEM result. All the above results demonstrated the occurrence of microphase separation during the preparation process of the ionogels. The microphase separation is induced by the moderate compatibility between the copolymer and IL. Specifically, the supersaturation of elastomeric matrix with a liquid would lead to uniform microphase separation while the matrix elasticity stabilizes the microstructure.[43] In our system, numerous noncovalent bonds exist between the PVDF-co-CTFE and the EMIMTFSI including hydrogen bonds and ion-dipole interactions (Figure S6).[44]

These strong physical interactions ensure the encapsulation of IL within the polymer networks, preventing the leakage of IL which in return enhances the stability of the PIG.

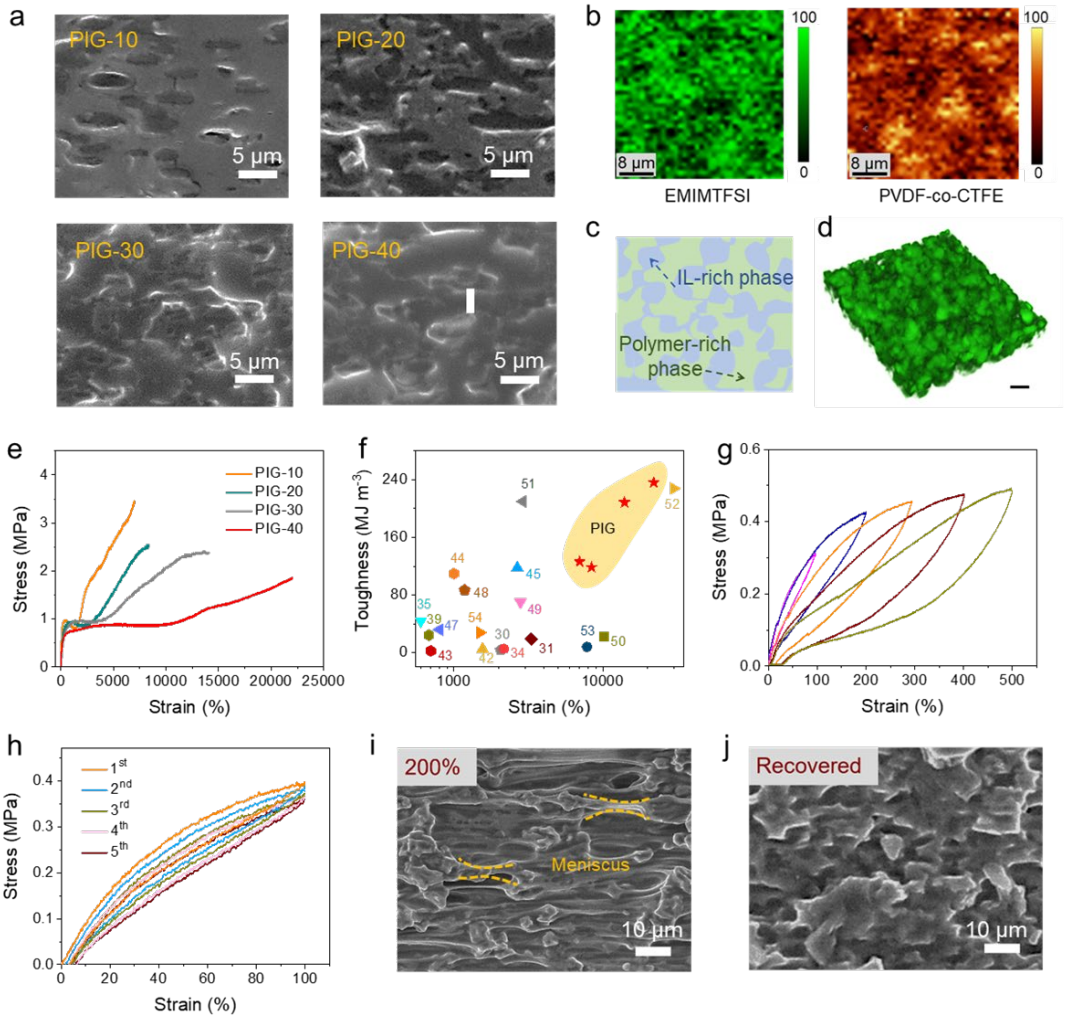

Figure 2. Morphology and mechanical properties of the PIG. (a) Section view SEM images of PVDF-co-CTFE, PIG-10, PIG-20, PIG-30, and PIG-40 samples. (b) Raman mapping images of PIG-40, indicating the distribution of the bicontinuous phases. (c) Schematic illustration of the biphasic structure of the PIG with IL-rich phase as continuous ion transport channels. (d) 3D confocal reconstruction of the bicontinuous structure (IL-rich phase). Scale bar: 20 μm. (e) Tensile stress–strain curves of PIG with different IL contents. (f) Comparison between this work and other high-performance gels in terms of strain and toughness. The data used are summarized in Table S3. (g) Representative cyclic stress-strain curves of PIG-40 at strains ranging from 100% to 500%. (h) Consecutive cyclic stress–strain curves of PIG-40 at a strain of 100% without intervals. Section view SEM images of PIG-40 under 200% strain (i), and immediately recovered from 200% strain (j).

Figure 2e showed that the increase in IL content would lead to higher stretchability due to liquid-induced plasticizing effect. This effect was confirmed by the decrease of glass transition temperature with the addition of IL (Figure S7). Interestingly, the PIG exhibited strain stiffening behavior where the addition of IL lead to synergistical promotion in mechanical strength and stretchability. Specifically, pure PVDF-co-CTFE had a maximum strain and ultimate strength of 3300% and 1.45 MPa (Figure S8), respectively, while those values for PIG-10 were significantly promoted to 7000% and 3.45 MPa, respectively. This phenomenon can be ascribed to the enhanced strain stiffening of ultrastretchable PIG compared to PVDF-co-CTFE film, and the liquid inclusion-induced stiffening effect (Figure S9).[45] When the IL content reached 40 wt%, the ionogel exhibited a super-stretchability of over 22000%, and at the same time, the measured tensile strength was still as high as 1.8 MPa. Since there was inevitable shrinkage of cross-sectional area at such a large strain, the corrected true tensile strength would better represent the actual stress of the ionogel. Remarkably, the value can reach as high as 407 MPa (Figure S10). Consequently, our PIG had superior toughness. The toughness of composites significantly increased from 31.8 MJ cm^{-3} for pure polymer to 236.3 MJ cm^{-3} for PIG-40 (Figure S11). We then compared the stretchability and toughness of the as-fabricated PIG with previous stretchable and tough gels such as phase-separated hydrogels and tough ionogels, our materials were mechanically superior to these reported high-performance ionic conductors (Figure 2f).[30-31, 34-35, 40, 46-55] Moreover, the Young's modulus of the PIG-40 was calculated to be ~1.1 MPa, which is comparable with human skin (0.5 - 1.95 MPa), indicating its feasibility for the development of skin-like wearable devices.

Elasticity is an essential parameter for ionogels, especially for their applications in stretchable electronics. However, most ionogels had poor elasticity, producing non-repeatable responses to deformation at strains higher than 50-100%. Here, cyclic tensile tests were conducted to study the elasticity property of the PIG. As demonstrated in Figure 2g, under predetermined strains, the loading-unloading curves of PIG-40 showed a small hysteresis loop and a negligible residual strain at strains of 100% and 200%. With increase in tensile strain, both the hysteresis area and residue ratio of the curves increased, which can be attributed to the energy dissipation effect of the rich noncovalent interactions within the ionogel (Figure S12). However, a residual strain of only 29% out of a strain at 500% was recorded, demonstrating the highly elastic nature of PIG-40. In contrast, the pure polymer showed a significantly large hysteresis loop and residual strain (27% at a strain of 200%) (Figure S13). The elasticity of PIG was further investigated by performing successive loading-unloading cycles at a strain of 100% (Figure 2h). Impressively, the curves almost overlapped with relatively constant residual strains, which gives evidence for the excellent resilience and fatigue resistance of the PIG-40. At high strain of 500%, PIG-40 can hardly recover immediately. However, it showed fast recovery capability. The recovery efficiency (defined in terms of tensile strength) of PIG-40 could achieve almost 100% within 10 min at 500% strain (Figure S14).[30] In addition, such good resilience can also be verified in the compressive test (Figure S15). This enhancement in resilience can be attributed to the structural effect of the bicontinuous network. During deformation, numerous menisci would form on the interface of the two phases (Figure S16a), offering an extra resilience force to facilitate the recovery of the stretched ionogles to its original state. Consequently, the ionogel can immediately recover from a 200% strain (Figure 2i and 2j).

However, upon large strain such as 1000%, the meniscus can be fully stretched with irreversible damage and therefore cannot provide the extra force to recover (Figure S16b).

Electrical and resistive sensing properties of PIG

In the biphasic ionogels, the continuous IL-rich phase provides effective ionic transport channels to promote their electrical conductivity (Figure 2c). The ionic conductivity of the PIG-10, PIG-20, PIG-30, PIG-40 and PIG-50 at 25 ºC were measured to be 1.9×10^{-7}, 7.2×10^{-7}, 7.1×10^{-6}, 3×10^{-5}, and 8.5×10^{-5} S cm^{-1}, respectively (Figure 3a and S17). By increasing the IL contents, the ionic conductivity of the ionogels increased by two orders. As a typical demonstration, PIG-40 was used as wire to connect a light-emitting diode (LED) to form a closed-circuit. As depicted in Figure 3b, when the ionogel was stretched, the brightness of the LED showed a little decrease and can be recovered rapidly after removing the strains, indicating good elasticity and electric responsiveness of the ionogel.

Figure 3c depicted the relative change in electrical resistance ($\Delta R/R_0$) as a function of strain (ε) for PIG-40. The parameter of gauge factor ($(\Delta R/R_0)/\varepsilon$) was used to evaluate the sensitivity of the sensor. The curve in Figure 3c gave two different slopes of 0.3 (region a) and 0.7 (region b), corresponding to the strain of 0-400% and 400-1000%, respectively. This sensing performance is comparable with the previously reported ionogel-based strain sensors (Table S4). We then performed the successive cyclic stretching and releasing test to observe the evolution of $\Delta R/R_0$ with increased strains. The results in Figure 3d indicated that the resistance of the PIG-40 can respond to various strains accurately and reversibly. In addition, the device showed consistent changes in $\Delta R/R_0$ during 1000 uninterrupted tests at a strain of 100%,

revealing the high reliability and durability of the I-skin (Figure 3e). We attribute this excellent stability to the high elasticity of the I-skin that allows it to reconfigure and recover from the structural deformations rapidly. The sensor can also respond to strain stably at frequencies ranging from 0.1 to 0.4 Hz (Figure S18). Interestingly, when the I-skin was pre-stretched to 500% strain, its sensitivity would be significantly enhanced, indicating the adaptive sensing property which may benefit specific applications (Figure 3f).

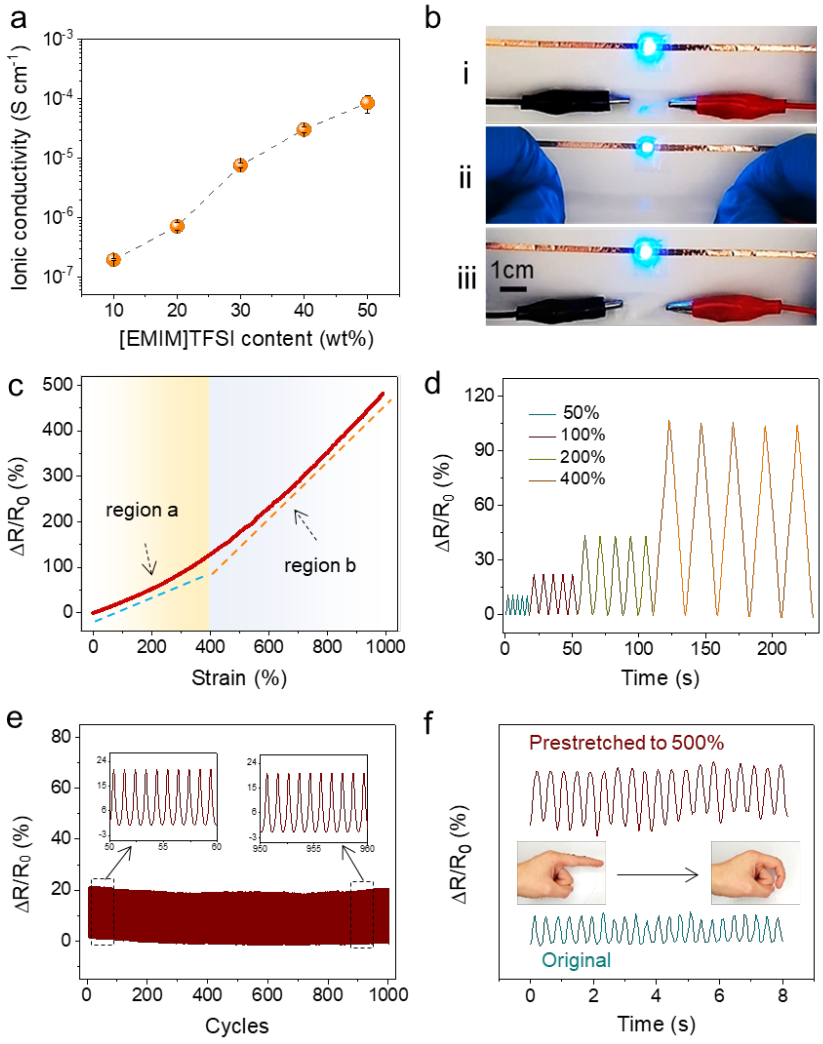

Figure 3. Electric properties of the PIG and their application as strain sensitive I-skin. (a) Influence of IL contents on the ionic conductivity of PIG. (b) Photographs of electrical circuits consisting of PIG-40 and LED. Relative resistance changes of I-skin as a function of strain (c) and at certain strains (50, 100, 200, 300, 400, and 500%) (d). (e) Relative change in resistance

under repeated loading-unloading processes at a strain of 100% for uninterrupted 1000 cycles. (f) The change in resistance of I-skin in original and pre-stretched state.

Multimodal sensing performance and mechanism

Although the I-skin can respond to mechanical deformation sensitively in resistance mode, such sensing mechanism needs extra energy supply and mismatches with biological perception mechanism which transform external stimuli into biopotential signals by means of ions as information carriers. Here, the stimuli-electricity conversion ability of the I-skin was studied to confirm its potential in self-powered sensing. As shown in Figure 4a, a sustained voltage was recorded upon a step compression of 40 kPa. The I-skin showed a quick response to external pressure. The generated voltage can stably keep as the pressure lasting, indicating its potential for mimicking the slow adapting receptor of the biological skins to detect static or low-frequency dynamic mechanical stimuli. After the initial stage, the voltage showed a slow decrease which can be attributed to the counterions. The pressure-voltage feature of the PIG-based I-skin can be evaluated by pressure sensitivity which defined as $S_p = \Delta V/\Delta P$, where ΔV and ΔP represent the variation in voltage and applied pressure, respectively. Figure 4b showed a linear response of voltage output up to a pressure of 300 kPa, allowing the skin to detect various pressures accurately. Specifically, at a pressure lower than 10 kPa, the pressure sensitivity of the I-skin is as high as 0.53 mV/kPa which can be ascribed to the moderate modulus of the I-skin. Upon large pressures, the I-skin can also deliver a high gauge factor of 0.2 mV/kPa which outperforms the state-of-art self-powered sensors (Table S5).[56] The I-skin can output repeatable voltage signals when applied a cyclic loading of 15 kPa, indicating the pressure-voltage transduction was reversible and stable (Figure 4c).

A force applied on the I-skin would cause transient stress distribution built within the ionogel which gives driving force to evoke the ion diffusion (Figure 4d and 4e). We assume that the cations and anions have different interactions with the copolymer matrix to mediate the ion diffusion during operation. Density functional theory (DFT) calculations were performed to evaluate the ion-polymer interactions. The geometry configurations were optimized and the average binding energy of $EMIM^+$ and the copolymer was calculated to be 14.27 kcal mol^{-1}, while the value for $TFSI^-$ and the copolymer was only 12.051 kcal mol^{-1} (Figure S19). This interaction difference was also confirmed by molecular dynamic (MD) simulation (Figure S20c). Meanwhile, anion has a higher diffusion coefficient than that of cation (Figure S20d). Consequently, the more mobile anions would undergo less dragging from the polymer matrix while the less mobile cations remain retention around the polymer matrix under compression. This preferential diffusion of the anions over cations would lead to a change in the spatial distribution of ions across the ionogel, yielding a self-induced potential between electrodes, which is referred to piezoionic effect (Figure 4e).[57] When the external compression was removed, the ion diffusion differences would gradually re-balance, making the output voltage drop to zero (Figure 4a). We then replace the EMIMTFSI by other ILs such as $OMIMBF_4$ and $OMIMPF_6$ to further investigate the effect of ions. The voltages were lower than that with EMIMTFSI, which can be attributed to the size effect in contribution of the power generation (Figure S21).[58] Meanwhile, with $OMIMPF_6$, the duration is low, which is similar to the rapid-adapting sensing of the human skin, indicating our I-skin can work as both rapid- and slow-adapting mechanoreceptors.

The high pressure-detection resolution of the I-skin enables it to monitor the mechanical movement of human body in a self-powered manner. Figure 4f shows the detection of subtle vibrations caused by vocal cord vibration. The I-skin is capable of monitoring and distinguishing sentences of “OK”, “Hello”, “Nice to meet you” and actions of cough and swallow. We then developed a fully integrated 4-by-4 sensor array for self-powered position detection (Figure S22). The ionogel was sandwiched by two encapsulation layers of PVDF-co-CTFE film. The whole device is transparent because the wires and the sensor unit in the device were all made from the ionogel. The sensor array can detect a single touch with a voltage output of ~8 mV (Figure S22c). Meanwhile, the distribution of generated voltage by each sensor under similar stimuli is uniform, indicating its high reliability (Figure S22d). Moreover, the array can detect multitouch. Specifically, when we press three sensor units at different positions simultaneously, the corresponding units can output similar voltage signals, while the crosstalk of the adjacent units was negligible (Figure S22e).

Except pressure, the I-skin can also detect mechanical deformation caused by stretching. As shown in Figure 4g, upon stretching, a voltage was yielded which gradually increased to a platform and remained relatively stable during operation. The output voltage can be improved by increasing the strain. Figure 4h showed a linear voltage-strain relationship, indicating its capability to respond to and recognize various strains. The stretch sensitivity of this I-skin can be defined as $S_s = \Delta V/\varepsilon$, which delivered a value of ~37 mV per 100% strain. As shown in Figure 4i, the sensor that is directly attached to the back of index finger can quantify the bending amplitude, and the generated voltage increased with larger bending angles. Furthermore, the

monitoring of such motion is stable and repeatable, indicating its high level of reliability as wearable devices.

The I-skin also showed the ability to detect temperature of objectives by generating thermo-diffusion potential.[59] As shown in Figure 4j, when an objective with temperature of 43 °C contacted the top of the I-skin, a voltage responded to the temperature stimulus and then the response gradually increased to the peak. When the temperature stimulus was removed, the voltage response dropped first and decreased slowly to the initial state.[56] The voltage output is also showed a linear relationship with temperatures. The temperature sensitivity was defined by the Seebeck coefficient of $S_T = \Delta V/\Delta T$, where ΔT is the temperature change. The I-skin showed a relatively high sensitivity of 0.26 mV/K at temperature lower than 40 °C, and the sensitivity increased to 1.06 mV/K for temperatures higher than 40 °C, which outperforms the existing technologies (Figure 4k and Table S5).[60] The increase of sensitivity at promoted temperatures can be attributed to the high mobility of anions. In addition, the temperature sensing ability is also stable and repeatable (Figure 4l). This feature greatly broadens the potential uses of the I-skin, equipping the device with a human-like ability to perceive in multiple dimensions.

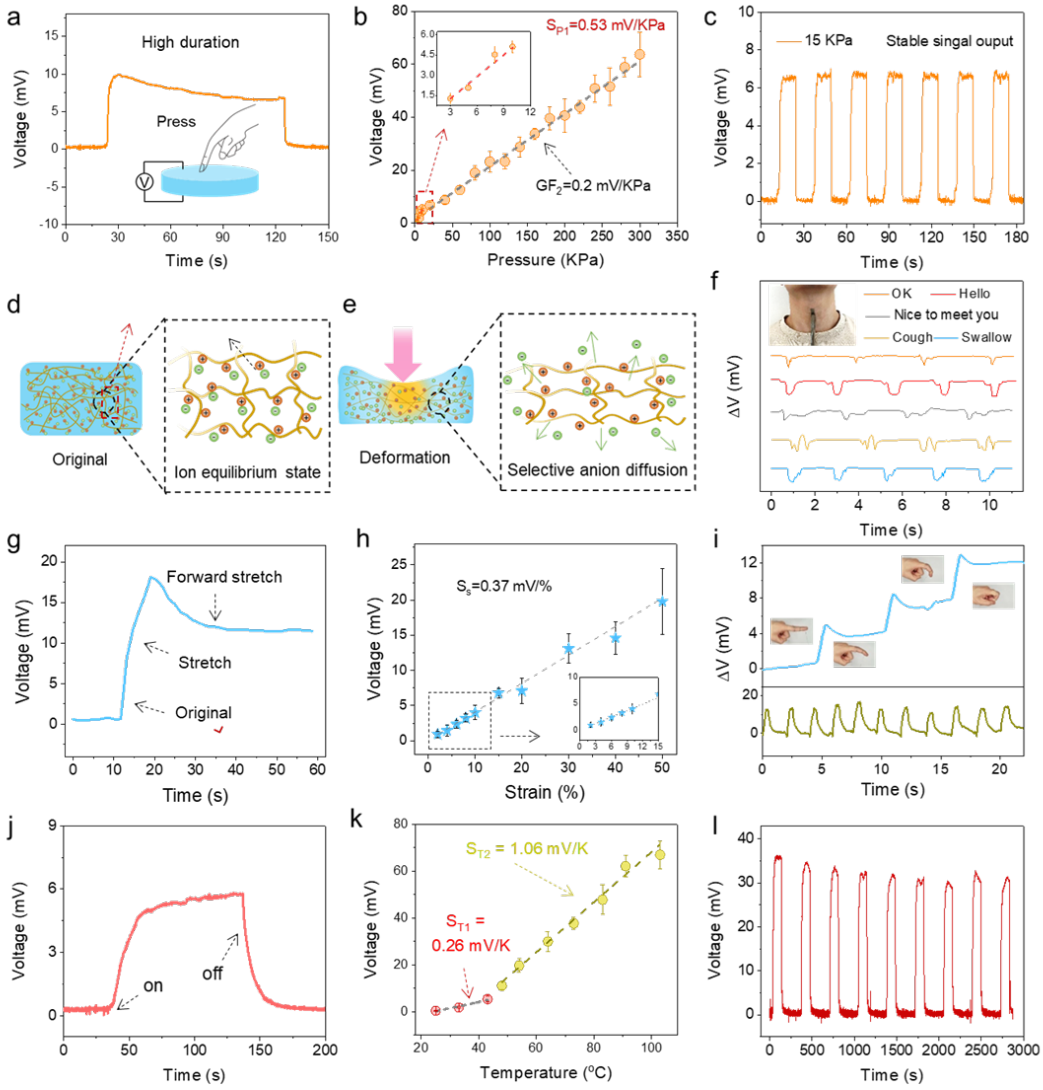

Figure 4. Multimodal sensing performance of the self-powered PIG-based I-skin. (a) Voltage output of the I-skin upon step compression at 40 kPa. (b) Voltage generated as a function of applied compression pressures. (c) Voltage output of the I-skin under consecutive compression at 15 kPa. (d) Distribution of ionic components in I-skin in equilibrium. (e) Schematic illustration of selective anion transport within the I-skin upon stimuli. (f) Real-time monitoring of human shallow breath, deep breath, and cough, respectively. The inset shows the electronic skin attached to volunteer's throat. (g) The relative output voltage of I-skin in response to a 30% strain. (h) Voltage generated as a function of applied strains. (i) Voltage response of the wearable sensor to different finger curvatures (up) and voltage in response to repeated fully bending of the finger (down). (j) Voltage output of the I-skin in response to temperature of 43 °C. (k) Voltage generated at various temperatures. (l) Voltage output of the I-skin when consecutively contacting temperature of 60 °C.

Stability of the PIG-based I-skin

Environmental tolerance is critical for I-skin to expand their applications in various conditions. The thermogravimetric analysis recorded a starting decomposition temperature up to ~400 °C for PIG-40, indicating its excellent thermal stability (Figure 5a). Dynamic temperature sweep measurement showed a high thermal-mechanical stability, indicating the ionogel structure is not destroyed at high temperature which due to the stable chemical cross-links in the ionogel (Figure 23). When stored at ambient condition or high temperature of 100 °C for up to ten days, PIG-40 can maintain its weight without obvious loss, indicating the absence of IL leakage (Figure 5b). PIG-40 also showed high size stability at various high temperatures from 0-100 °C (Figure 24). Moreover, PIG-40 PIG-40 can be reversibly twisted or bent without fracture at -20 °C, revealing good elasticity of the ionogel at sub-zero temperatures (Figure 5c). The ionogel displayed good hydrophobicity with a water contact angle of 103° (Figure S25). This hydrophobicity can be attributed to the hydrophobic nature of the IL and polymer. With such property, the PIG was insensitive to moisture with a weight increase of ~1% even at very high humidity (Figure S26). Except water, the ionogel also showed good resistance to many organic solvents (Table S2). All the above results confirmed that the PIG can maintain function in various harsh conditions which is essential for practical applications. Moreover, the ionogels can be easily recycled due to the existence of reversible physical crosslinking and noncovalent bonds.[61-62] As depicted in Figure S27, PIG-40 can be easily dissolved in EA to get a homogenous solution which can be reprocessed by solvent evaporation to obtain transparent ionogels with remained properties (Figure 5d).

With high environmental stability, the I-skin can work under various conditions. For instance, the I-skin can function effectively in submerged aqueous environment (Figure 5e and 5f). In

addition, the I-skin can maintain its response when being placed in scorching outdoor environment. We tested the response of the I-skin to the same stimuli of 100 g weight at both indoor and outdoor environments. Figure 5g demonstrates that the I-skin can produce consistent voltage signals, showcasing its stability in environments where most hydrogel-based sensors would fail due to significant water loss. In addition, the I-skin showed excellent durability and outstanding long-term stability. Figure 5h showed that the I-skin can maintain stable responses under repeated loading and unloading of 80 kPa pressure for more than 600 cycles even with a long-term storage of 3 months.

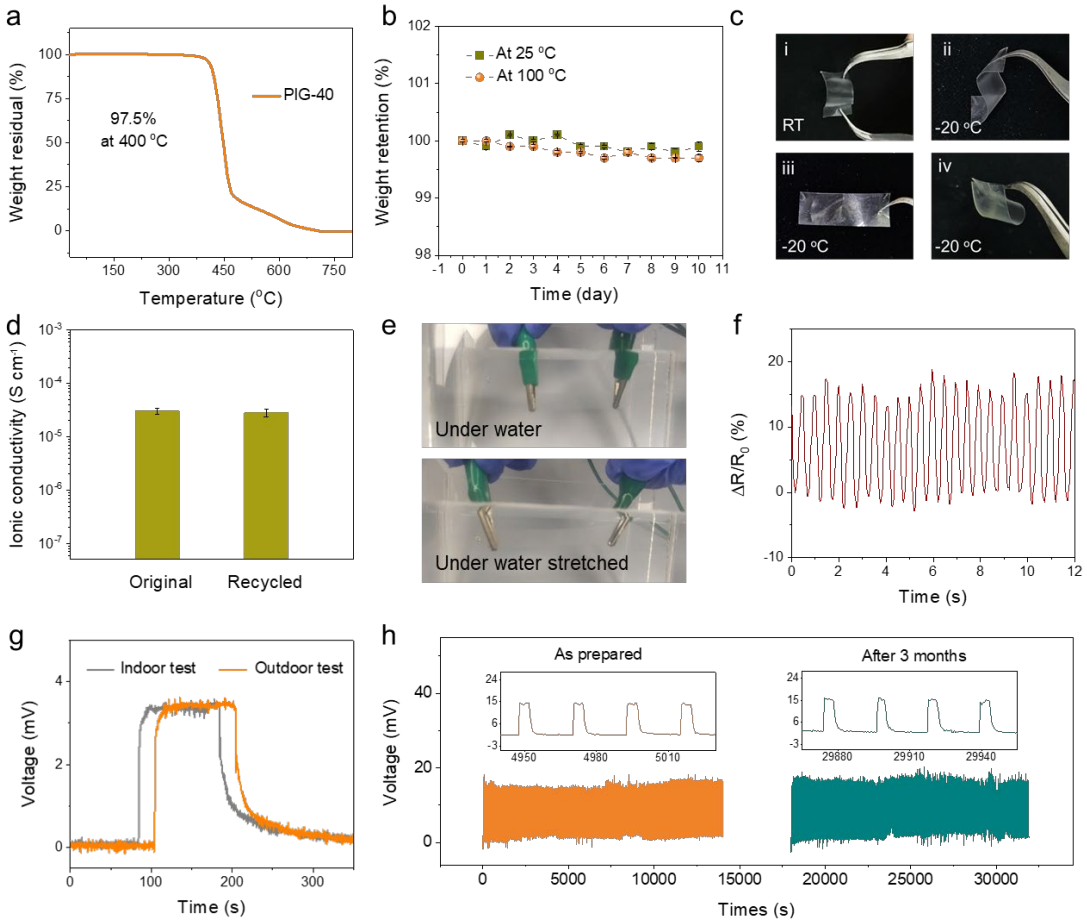

Figure 5. Environmental stability of the PIG-based I-skin. (a) TGA of PIG-40. (b) The weight retention/loss test of PIG-40 stored at 25 ºC and 100 ºC for ten days. (c) Photos showing PIG-40 samples being bent or twisted at 25 °C and -20 °C. (d) Ionic conductivity of the original and recycled PIG-40. (e) PIG-based I-skin being placed under water. (f) Strain sensing of I-

skin under water. (g) Voltage output response to a 100 g weight on I-skin at both indoor and outdoor environments. (h) Voltage output of PIG-40 (before and after storage in the ambient conditions for 3 months) under repeated loading/unloading of 80 kPa pressure of 600 cycles.

Simultaneous monitoring of multiple stimuli by ML

The PIG-based I-skin achieves sensitive sensing of pressure and temperature, respectively, and generates electrical responses with distinct voltage patterns. However, two stimuli (pressure and temperature) applied on the I-skin simultaneously induce the hybrid and complex response signal of voltage. For example, as shown in Figure 6a, a pressure of 0.5 N and a temperature of 78.3 °C contribute to a voltage response of 46.8 mV, while 5.6 N and 26.6 °C give rise to a response of 21 mV. Nevertheless, it is worth noting that the highly coupled response behavior still inherits the characteristic patters of individual stimuli. For instance, pressure induces a transient voltage response (rapid-adapting response), while the subsequent slow variation of voltage corresponds to a typical temperature response behavior. In addition, the electrical signal of the I-skin drops and gradually returns to the initial state (base line) when the two stimuli are withdrawn, which suggesting the stationarity of the sensing signal of the I-skin.

The voltage response can reflect the variation of each stimulus in detail, and the local dependence on the stimulus is stable, which allow us to inversely infer the stimuli from the voltage signal. Previous studies have shown that the mixed signal can be decoupled and identified by machine learning (ML).[63] We then designed a ML decoupling model to disentangle the voltage, which consists of four sets of Long Short-Term Memory (LSTM) layers followed by Layer Normalization, designed to extract features from sequential data (Figure 6b). We delve into the detailed calculations of LSTM and Layer Normalization operations, followed by a single fully connected layer. We will conclude by discussing the

computation of the Mean Squared Error and Mean Absolute Error loss functions and the backpropagation process for weight updates (details in Note and Figure S28, Supporting Information).

Based on this well-trained ML decoupling model, the I-skin is capable of monitoring real-time changes of the two stimuli (pressure and temperature) simultaneously. As shown in Figure 6c, when irregular pressure (0-6 N) and temperature (22-110 °C) are applied to the I-skin at the same time, the voltage signal of the I-skin can be decoupled into the pressure and temperature, which are in good agreement with the measured values. Furthermore, during 15130 time steps of multimodal coupled training, the mean absolute error of the predicted values for the two stimuli decoupled from the voltage signals are only 0.17 N (pressure) and 1.3 °C (temperature) for each step, which indicates the high accuracy of the decoupled signals. As a result, the specific hybrid and mixed signals can be accurately identified for each stimulus, enabling simultaneous monitoring of multiple stimuli by the single I-skin. As a demonstration, the I-skin can sense the pressure and temperature applied by a finger (Figure 6d). When the index finger (temperature of ~36 °C, Figure 6e) applied a pressure of 2.67 N onto the I-skin, a voltage of 19.5 mV was generated. This voltage can be decoupled into a temperature of ~36.3 °C and a pressure of 2.7 N, which is highly consistent with the experimental measurements (Figure 6f).

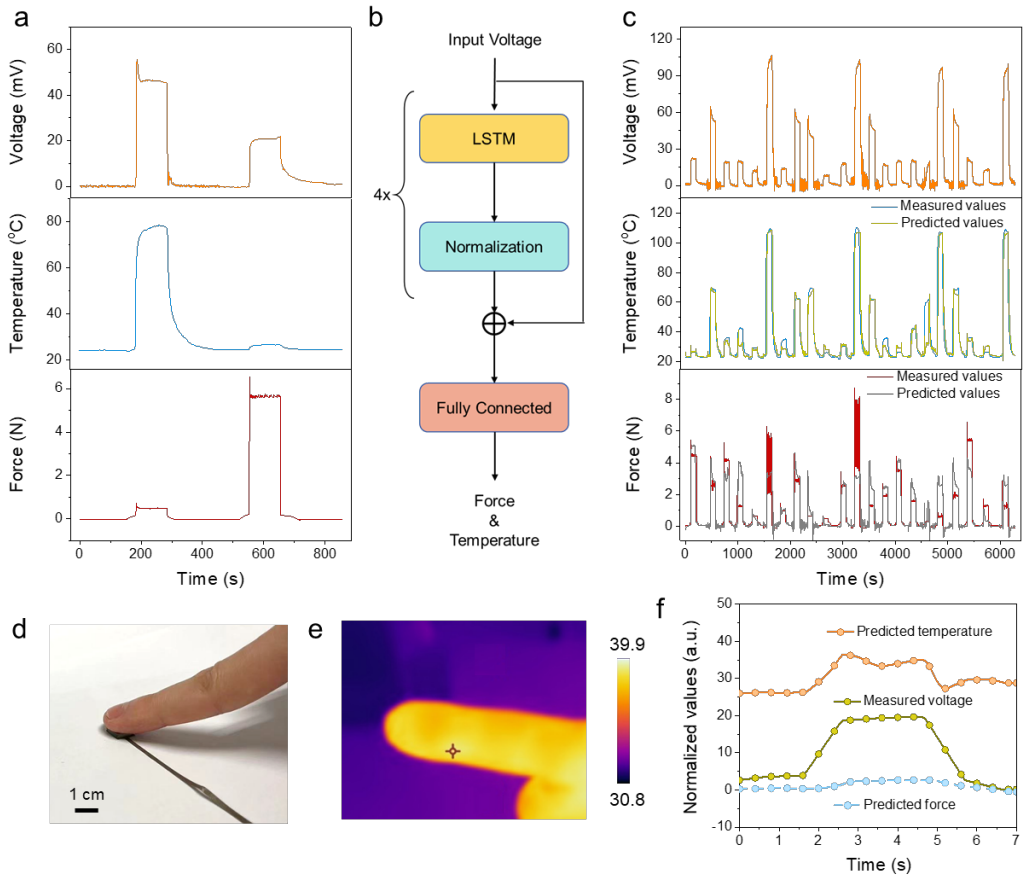

Figure 6. Decoupling analysis and the application of I-skin. (a) Electrical response of the I-skin with simultaneous pressure and temperature stimuli. (b) The architecture of the ML decupling model. (c) The predicted values for pressure and temperature based on I-skin potential response signals and the measured values for voltage response and each stimulus. (d) Photos showed the index finger pressed on I-skin. (e) Thermal image of the index finger. (f) Simultaneous monitoring of finger pressure and temperature using I-skin.

Conclusion

In summary, inspired by biological skins, we reported an I-skin with multimodal stimuli-electricity conversion by polyvinylidene fluoride copolymer-based ionogel featured at ultrastretchability, excellent elasticity, high reliability, and good environmental stability. The microphase-separated bicontinuous structure of PIG can effectively dissipate energy during deformation and promote stretchability, elasticity, and strength simultaneously. The ionogel-based I-skin can respond to various stimuli including strain, pressure, and temperature by self-

induced potential. The I-skin can stably respond to external stimuli with high sensitivity (e.g., ~37 mV per 100% strain, 0.53 mV/kPa and 1.06 mV/K for strain, pressure, and temperature sensing, respectively), which outperformed the existing technologies. Simultaneous perception and monitoring of pressure and temperature is achieved through decoupling the voltage signal of the I-skin by ML model. We believe the design of microphase-separated I-skin developed in this study can be extended to the creation of variety of I-skins with wide tunability, high sensitivity and self-powered capability. Further efforts will be focused on realizing precise control of phase separation, achieving skin-like self-healing ability and promoting the sensitivity of the I-skin.

Acknowledgments

D. Lv, and X. Li. contributed equally to this work. This work was financially supported by the Research Grant Council of Hong Kong (No. CityU 11305219, 11307220), Collaborative Research Fund (CRF) Hong Kong (C1006-20WF), and Shenzhen Basic Research Program (JCYJ20210324134009024).

Experimental section

Materials

The ILs of EMIMTFSI, $EMIMBF_4$, OMIMCl, $OMIMBF_4$, OMIMTFSI and $OMIMPF_6$ were purchased from Sigma-Aldrich. The PVDF-co-CTFE was obtained from the Institute of Chemical Material, Mianyang, PR China. Solvent of EA was purchased from Sigma-Aldrich. All chemicals were used as received.

Preparation of PIG

The PVDF-co-CTFE was first dissolved in EA to obtain a homogenous solution with a weight ratio of 5 wt%. Then different content of ILs (with a loading of 10 - 50 wt% in the mixture) was added to the as-prepared solution and the mixture was continuously stirred for 2 h. Afterwards, the mixture was poured into a glass mold, followed by solvent evaporation at ambient condition (25±4 ºC, *RH* 50±15%) for ~3-5 days to obtain a dried and transparent film. Finally, the obtained film was further dried in a vacuum oven at 60 ºC for 48 h to remove solvent residue.

Characterizations

The morphology study of the ionogels was performed using field emission SEM (Philips XL30CP) at 10.0 kV. The optical photos were taken with a camera (Nikon D5500). The size stability of PIG was tested by take photos of PIG -40 after heating at various temperature for one hour. Optical transmittance values were measured by ultraviolet-visible spectroscopy (UV-Vis). Confocal fluorescence microscopy image of the PIG was obtained by a Nikon Ti ECLIPSE inverted optical microscope. The ionogel was stained with fluorescein isothiocyanate (520 nm dye) of green fluorescence to observe the distribution of IL. Attenuated total reflectance infrared (ATR-IR) spectrums were obtained by a PerkinElmer Spectrum 100 instrument that equipped with ATR accessories. The Raman scattering analysis and 2D Raman mapping were recorded on a Raman spectroscopy (WITec alpha300 access) using laser with a wavelength of 532 nm. The thermogravimetric analysis (TGA) of the ionogel was tested by a TA Q600 differential thermal analyzer with a heating rate of 10 ºC min^{-1}. Differential scanning calorimetry (DSC) measurements were conducted by a TA DSC25 instrument with a temperature range from -80 °C to 100 °C with a heating speed of 10 °C min^{-1}. The rheological

characteristics and viscosity were measured with a rotational rheometer (Malvern Kinexus Lab+). The rotating top plate was 15 mm in diameter. Dynamic temperature sweep measurements at an angular frequency of 1 Hz were conducted from 20 to 100 °C with a heating rate of 5 °C/min. The frequency sweep measurements at room temperature were conducted from 0.1 to 100 Hz. The mechanical tests including stretching and compression of the ionogels were conducted by an Instron 5566 instrument (Chatillon Force Test). Tensile experiments were conducted at ambient temperature at a strain rate of 10 mm min^{-1} for both stretching and relax rate. The electrical characterizations including resistance and voltage were recorded using a Keithley 6500 source meter. The ionic conductivity of the ionogels was measured by an Ivium-n-Stat (Ivium Technologies B.V., Eindhoven, The Netherlands) at room temperature (contact area 0.785 cm^2). The ionic conductivities were calculated by: $\sigma=d/RA$, where d, R and A are the thickness, resistance and contact area of the ionogels, respectively. For all the mechanical and electrical characterizations, three repeated tests were conducted to examine the data reproducibility. Error bars were added to the figures by calculating the standard deviation of the corresponding data.

Electric measurement of the I-skin

Thin silver electrodes were used for the preparation of the I-skin. The performance tests of the I-skin including the resistance change upon stretching, voltage output upon stimulus such as strain, pressure and temperature were conducted by combing the Keithley 6500 source meter and the Instron 5566 instrument. The size of I-skin used for strain sensing is 50×8×0.5 mm (length, width, and thickness) while the size of I-skin used for pressure and temperature sensing is 8×8×4 mm. The performances of the I-skin under various harsh conditions including low

temperature of -20 °C, submerged aqueous environment, and outdoor environment were recorded by placing the I-skin in refrigerator, under water and outdoor environments, respectively. Experiments with human subjects: The experiments with human subjects were performed in compliance with all the ethical regulations under a protocol that was reviewed and approved by the JCC College Human Ethics Sub-committee of City University of Hong Kong (Jcc2324ay001).

References

[1] Y. Wu, Y. Liu, Y. Zhou, Q. Man, C. Hu, W. Asghar, F. Li, Z. Yu, J. Shang, G. Liu, *Sci. Robot.* **2018**, *3*, eaat0429.

[2] M. Jin, S. Park, Y. Lee, J. Lee, J. Chung, J. Kim, J. Kim, S. Kim, E. Jee, D. Kim, *Adv. Mater.* **2017**, *29*, 1605973.

[3] Z. Lei, Q. Wang, S. Sun, W. Zhu, P. Wu, *Adv. Mater.* **2017**, *29*, 1700321.

[4] S. Hajra, S. Panda, H. Khanberh, V. Vivekananthan, E. Chamanehpour, Y. K. Mishra, H. J. Kim, *Nano Energy* **2023**, *115*, 108729.

[5] Q. Hua, J. Sun, H. Liu, R. Bao, R. Yu, J. Zhai, C. Pan, Z. Wang, *Nat. Commun.* **2018**, *9*, 244.

[6] G. Ge, Y. Zhang, J. Shao, W. Wang, W. Si, W. Huang, X. Dong, *Adv. Funct. Mater.* **2018**, *28*, 1802576.

[7] S. N. Faisal, T.-T. N. Do, T. Torzo, D. Leong, A. Pradeepkumar, C.-T. Lin, F. Iacopi, *ACS Appl. Nano Mater.* **2023**, *6*, 5440.

[8] Y. Yu, J. Li, S. A. Solomon, J. Min, J. Tu, W. Guo, C. Xu, Y. Song, W. Gao, *Sci. Robot.* **2022**, *7*, eabn0495.

[9] D. Son, J. Kang, O. Vardoulis, Y. Kim, N. Matsuhisa, J. Oh, J. To, J. Mun, T. Katsumata, Y. Liu, A. McGuire, M. Krason, F. Molina-Lopez, J. Ham, U. Kraft, Y. Lee, Y. Yun, J. Tok, Z. Bao, *Nat. Nanotechnol.* **2018**, *13*, 1057.

[10] G. Li, S. Liu, L. Wang, R. Zhu, *Sci. Robot.* **2020**, *5*, eabc8134.

[11] Y. Liu, K. He, G. Chen, W. Leow, X. Chen, *Chem. Rev.* **2017**, *117*, 12893.

[12] M. Ho, Y. Ling, L. Yap, Y. Wang, D. Dong, Y. Zhao, W. Cheng, *Adv. Funct. Mater.* **2017**, *27*, 1700845.

[13] E. D'Elia, S. Barg, N. Ni, V. Rocha, E. Saiz, *Adv. Mater.* **2015**, *27*, 4788.

[14] J. Sun, C. Keplinger, G. Whitesides, Z. Suo, *Adv. Mater.* **2014**, *26*, 7608.

[15] C. Yang, Z. Suo, *Nat. Rev. Mater.* **2018**, *3*, 125.

[16] Y. Dobashi, D. Yao, Y. Petel, T. Nguyen, M. Sarwar, Y. Thabet, C. L. Ng, E. Scabeni Glitz, G. Nguyen, C. Plesse, F. Vidal, C. Michal, J. Madden, *Science* **2022**, *376*, 502.

[17] X. Pan, Q. Wang, D. Benetti, Y. Ni, F. Rosei, *Nano Energy* **2022**, *103*, 107718.

[18] C. C. Kim, H. H. Lee, K. H. Oh, J. Y. Sun, *Science* **2016**, *353*, 682.

[19] J. Y. Sun, X. Zhao, W. Illeperuma, O. Chaudhuri, K. Oh, D. Mooney, J. Vlassak, Z. Suo, *Nature* **2012**, *489*, 133.
[20] B. Yi, L. Ai, C. Hou, D. Lv, C. Cao, X. Yao, *ACS Appl. Mater. Interfaces* **2022**, *14*, 29315.
[21] J. Le Bideau, L. Viau, A. Vioux, *Chem. Soc. Rev.* **2011**, *40*, 907.
[22] Z. Luo, W. Li, J. Yan, J. Sun, *Adv. Funct. Mater.* **2022**, *32*, 2203988.
[23] Z. Shen, X. Zhu, C. Majidi, G. Gu, *Adv. Mater.* **2021**, *33*, 2102069.
[24] Y. Ren, J. Guo, Z. Liu, Y. Sun, L. L., F. Yan, *Sci. Adv.* **2019**, *5*, eaax0648.
[25] Z. Cao, H. Liu, L. Jiang, *Mater. Horizons* **2020**, *7*, 912.
[26] Y. Cao, T. G. Morrissey, E. Acome, S. I. Allec, B. M. Wong, C. Keplinger, C. Wang, *Adv. Mater.* **2017**, *29*, 1605099.
[27] Z. Wang, B. Yi, M. Wu, D. Lv, M. L. He, M. Liu, X. Yao, *Adv. Funct. Mater.* **2021**, *31*, 2102888.
[28] C. Hou, C. Cao, R. Ma, L. Ai, Z. Hu, Y. Huang, X. Yao, *ACS Appl. Mater. Interfaces* **2023**, *15*, 11379.
[29] Z. Lei, P. Wu, *Nat. Commun.* **2019**, *10*, 3429.
[30] L. Xu, Z. Huang, Z. Deng, Z. Du, T. Sun, Z. Guo, K. Yue, *Adv. Mater.* **2021**, *33*, 2105306.
[31] W. Li, L. Li, S. Zheng, Z. Liu, X. Zou, Z. Sun, J. Guo, F. Yan, *Adv. Mater.* **2022**, *34*, 2203049.
[32] K. Cui, T. Sun, X. Liang, K. Nakajima, Y. Ye, L. Chen, T. Kurokawa, J. Gong, *Phys. Rev. Lett.* **2018**, *121*, 185501.
[33] H. Qiao, S. Sun, P. Wu, *Adv. Mater.* **2023**, 2300593.
[34] H. Xiang, X. Li, B. Wu, S. Sun, P. Wu, *Adv. Mater.* **2023**, *35*, 2209581.
[35] M. Wang, P. Zhang, M. Shamsi, J. Thelen, W. Qian, V. Truong, J. Ma, J. Hu, M. Dickey, *Nat. Mater.* **2022**, *21*, 359.
[36] Y. Kim, H. Moon, *Adv. Funct. Mater.* **2019**, *30*, 1907290.
[37] R. Tamate, K. Hashimoto, T. Horii, M. Hirasawa, X. Li, M. Shibayama, M. Watanabe, *Adv. Mater.* **2018**, *30*, 1802792.
[38] Y. Cao, Y. Tan, S. Li, W. Lee, H. Guo, Y. Cai, C. Wang, B. C. Tee, *Nat. Electron.* **2019**, *2*, 75.
[39] H. Li, X. Li, N. Liu, D. Liu, Z. Wang, F. Chen, *Polymer* **2023**, *282*, 126166.
[40] J. Wang, B. Wu, P. Wei, S. Sun, P. Wu, *Nat. Commun.* **2022**, *13*, 4411.
[41] C. Cao, X. Huang, D. Lv, L. Ai, W. Chen, C. Hou, B. Yi, J. Luo, X. Yao, *Mater. Horizons* **2021**, *8*, 3399.
[42] S. Zheng, J. Tang, D. Lyu, M. Wang, X. Yang, C. Hou, B. Yi, G. Lu, R. Hao, M. Wang, Y. Wang, H. He, X. Yao, *Adv. Mater.* **2021**, *34*, 2106410.
[43] C. Fernández-Rico, S. Schreiber, H. Oudich, C. Lorenz, A. Sicher, T. Sai, V. Bauernfeind, S. Heyden, P. Carrara, L. Lorenzis, R. Style, E. Dufresne, *Nat. Mater.* **2023**, 1.
[44] S. Sharma, A. Chhetry, S. Zhang, H. Yoon, C. Park, H. Kim, M. Sharifuzzaman, X. Hui, J. Park, *ACS Nano* **2021**, *15*, 4380.
[45] R. Style, R. Boltyanskiy, B. Allen, K. Jensen, H. Foote, J. Wettlaufer, E. Dufresne, *Nat. Phys.* **2015**, *11*, 82.

[46] T. Li, Y. Wang, S. Li, X. Liu, J. Sun, *Adv. Mater.* **2020**, *32*, 2002706.
[47] K. Cho, S. An, D. Cho, J. Kim, J. Nam, M. Kim, K. Lee, *Adv. Funct. Mater.* **2021**, *31*, 2102386.
[48] P. Liu, D. Pei, Y. Wu, M. Li, X. Zhao, C. Li, *J. Mater. Chem. A* **2022**, *10*, 25602.
[49] X. Wang, Y. Wang, X. Yang, Z. Lu, Y. Men, J. Sun, *Macromolecules* **2021**, *54*, 10767.
[50] B. Zhang, X. Zhang, H. Song, D. Nguyen, C. Zhang, T. Liu, *ACS Appl. Mater. Interfaces* **2022**, *14*, 32551.
[51] D. Weng, F. Xu, X. Li, S. Li, Y. Li, J. Sun, *ACS Appl. Mater. Interfaces* **2020**, *12*, 57477.
[52] L. Zhang, Z. Liu, X. Wu, Q. Guan, S. Chen, L. Sun, Y. Guo, S. Wang, J. Song, E. Jeffries, C. He, F. Qing, X. Bao, Z. You, *Adv. Mater.* **2019**, *31*, 1901402.
[53] Y. Miwa, J. Kurachi, Y. Kohbara, S. Kutsumizu, *Commun. Chem.* **2018**, *1*, 5.
[54] Y. Ye, H. Oguzlu, J. Zhu, P. Zhu, P. Yang, Y. Zhu, Z. Wan, O. Rojas, F. Jiang, *Adv. Funct. Mater.* **2022**, *33*, 2209787.
[55] M. Hua, S. Wu, Y. Ma, Y. Zhao, Z. Chen, I. Frenkel, J. Strzalka, H. Zhou, X. Zhu, X. He, *Nature* **2021**, *590*, 594.
[56] M. Xia, N. Pan, C. Zhang, C. Zhang, W. Fan, Y. Xia, Z. Wang, K. Sui, *ACS Nano* **2022**, *16*, 4714.
[57] J. Lee, H. Choi, S. Kong, S. Park, D. Park, J. Kim, S. Kwon, J. Kim, S. Choi, S. Lee, *Adv. Mater.* **2021**, *33*, 2100321.
[58] D. Lv, S. Zheng, C. Cao, K. Li, L. Ai, X. Li, Z. Yang, Z. Xu, X. Yao, *Energy Environ. Sci.* **2022**, *15*, 2601.
[59] C.-G. Han, X. Qian, Q. Li, B. Deng, Y. Zhu, Z. Han, W. Zhang, W. Wang, S.-P. Feng, G. J. S. Chen, *Science* **2020**, *368*, 1091.
[50] Y. Wang, H. Wu, L. Xu, H. Zhang, Y. Yang, Z. Wang, *Sci. Adv.* **2020**, *6*, eabb9083.
[61] J. Zheng, S. F. D. Solco, C. J. E. Wong, S. A. Sia, X. Y. Tan, J. Cao, J. C. C. Yeo, W. Yan, Q. Zhu, Q. Yan, W. Jing, S. Ady, L. Zibiao, *J. Mater. Chem. A* **2022**, *10*, 19787.
[62] M. Liu, P. Liu, G. Lu, Z. Xu, X. Yao, *Angew. Chem. Int. Ed.* **2018**, *130*, 11412.
[63] N. Dai, I. Lei, Z. Li, Y. Li, P. Fang, J. Zhong, *Nano Energy* **2022**, 108041.

Entry for the Table of Contents

A microphase-separated bicontious ionogel is constructed to achieve skin-like mechanical properties such as high elasticity, ultrastretchability, and a Young's modulus similar to human skin. With abundant ion-polymer interactions and selective ion transport ability, the ionogel is applied as I-skin in response to diverse stimuli such as strain, pressure, and temperature sensitively, enabling multimodal sensing based on ion currents.

Dong Lv, Xin Li, Xin Huang, Chunyan Cao, Liqing Ai, Xuejiao Wang, Sai Kishore Ravi* and Xi Yao*

Microphase-separated elastic and ultrastretchable ionogel for reliable ionic skin with multimodal sensation